TENSILE TESTING OF SUB-SIZED 316L STEEL SPECIMENS IN LIQUID LEAD

K. TUČEK[1], Z. SZÁRAZ[1,2], R. NOVOTNÝ[1], M. KNAPEK[1,3], M. NOVÁK[1,4], D. MONIZ[1], K.-F. NILSSON[1], C. FAZIO[1]

[1] European Commission, Joint Research Centre, Petten, The Netherlands
[2] Present address: Slovak University of Technology, Faculty of Material Science and Technology, Trnava, Slovak Republic
[3] Charles University, Faculty of Mathematics and Physics, Department of Physics of Materials, Prague, Czech Republic
[4] University of Chemistry and Technology Prague, Department of Power Engineering, Prague, Czech Republic

Email contact of corresponding author: kamil.tucek@ec.europa.eu

Abstract

The influence of liquid lead on mechanical properties of austenitic stainless steel 316L(N) and its welds have been studied in the Joint Research Centre's (JRC's) LIquid Lead LAboratory (LILLA). LILLA allows testing of mechanical and corrosion properties of materials in liquid lead with controlled dissolved oxygen concentrations and at temperatures up to 650°C. The load is generated by pneumatic bellow-based devices. For the present study, 316L(N) sub-size flat and round tensile specimens from both the base metal and the 75 mm thick submerged arc welded (SAW) joint were prepared. Prior to tensile testing, polished specimens were pre-exposed in liquid lead at 500 °C for at least 30 h. During this phase, the oxygen content in liquid lead was maintained below 10^{-8} wt.% with the cover gas control system implemented in LILLA through flushing of Ar-H_2 mixture. Tensile tests were subsequently conducted both at 400 °C and 550 °C at initial strain rates of 5×10^{-5} s^{-1} and 5×10^{-6} s^{-1}, respectively. During all tensile tests, the content of oxygen dissolved in lead was continuously monitored and actively controlled to be below 10^{-8} wt.%. The results and post-test analyses have shown no evident impact of liquid Pb on the tensile properties and microstructure of the investigated steels and welds exposed to the above-described conditions. The paper briefly describes the observed results with respect to the literature data. This research supports resolution of key safety and licensing aspects related to structural materials and components for heavy liquid metal cooled fast reactor technology demonstrators considered in Europe, MYRRHA (with lead-bismuth eutectic coolant) and ALFRED (with lead coolant), and was embedded in the GEMMA Euratom Horizon 2020 collaborative project.

1. INTRODUCTION

The Lead cooled Fast Reactor (LFR) has been selected in Generation IV International Forum (GIF) as one of the six promising advanced reactor concepts. The use of liquid lead allows operation at close to atmospheric pressure, without the need to maintain robust structures to provide a pressure boundary. Lead is also chemically relatively inert in contact with air and water. A high boiling point of lead (1749°C) as well as high thermal inertia and natural convection characteristics further contribute to good passive safety features of LFRs [1].

In the context of the LFR technology, material behaviour in heavy liquid metals has historically been a main research topic. This paper first briefly describes activities of the European Commission, Joint Research Centre (JRC) in this domain. Outcomes of the slow-strain rate tensile (SSRT) tests conducted in Ar and liquid lead environment in the LILLA facility at the JRC Petten [2] are thereafter discussed. The research was in part performed in collaboration with partners within the GEMMA Horizon 2020 collaborative project [3]. Together with other GEMMA partner's results, the JRC data were used to provide some first recommendations for guidelines and design rules on how to incorporate environmental effects with respect to liquid lead to the RCC-MRx Design Code (Design and Construction Rules for Mechanical Components in high-temperature structures, experimental reactors and fusion reactors) [4].

2. JRC PETTEN ACTIVITIES RELATED TO STRUCTURAL MATERIAL INTEGRITY FOR LEAD COOLED FAST REACTORS

Safety and technology aspects related to material degradation in heavy liquid metals are at the forefront of the JRC's international collaborative efforts. These include:

— European Committee for Standardization (Comité Européen de Normalisation – CEN): The JRC coordinates Prospective Group 2 of the CEN Workshop 64, which aims at further development of the RCC-MRx Design Code for advanced reactor systems, considering, among others, licensing needs for heavy liquid metal cooled fast reactor technology demonstrators envisaged in Europe, MYRRHA (with lead-bismuth eutectic [LBE] coolant) and ALFRED (with lead coolant). Recently, two RCC-MRx Code Evolution and R&D proposals were developed with the JRC contribution on: (i) inclusion of environmental effects related to heavy liquid metal coolants in the Code (in cooperation with the Belgian Nuclear Research Centre [SCK•CEN]); and (ii) use of the small punch test (SPT) for design and health monitoring;

— Joint Programme on Nuclear Materials of the European Energy Research Alliance (EERA JPNM): In the frame of EERA JPNM, the JRC co-leads the Sub-Programme on pre-normative research (SP-A) concerning codes & standards, materials and component qualification. A key goal is to shorten time to qualify materials for operating conditions of the European Sustainable Nuclear Industrial Initiative (ESNII) demonstrators (incl. ALFRED LFR) and the MYRRHA research facility. The JRC contributed to several EERA JPNM strategic development documents, including the Vision Paper, Strategic Research Agenda [5], and Multi-Annual Work Plan. In the frame of the ORIENT-NM (Organisation of the European Research Community on Nuclear Materials) Horizon 2020 project, the JRC – together with other key partners in materials research – explores the possibility of establishing a Co-Funded European Partnership (CEP) on nuclear materials;

— Generation IV International Forum (GIF): Within the GIF LFR provisional System Steering Committee (pSSC), the JRC contributed to the drafting and updates of several safety-related documents which were prepared in the collaboration with the GIF Risk and Safety Working Group (RSWG) and addressed aspects related to lead-induced material degradation comprehensively. This included the LFR System Safety Assessment document (issued in 2020 [1]) and the LFR-specific Safety Design Criteria (published in 2021 [6]). In parallel, the JRC contributes to the GIF Advanced Manufacturing and Materials Engineering (AMME) Task Force, which aims at reducing the time to deployment of advanced reactor systems by, among others, promoting agility in codes and standard development, and sharing of practices for design optimizations;

— OECD Nuclear Energy Agency (NEA) Expert Group on Reactor Coolants/Components Technology: The JRC actively participates in the work of the Expert Group with the contribution to the State-of-the-art Report on the liquid metal environmental effects on materials for liquid metal cooled reactors. In this context, the JRC Petten specifically contributes to drafting of sections related to: (a) description of the LFR system; and (b) identification of main needs to support the development of Design Codes (RCC-MRx).

The JRC Petten has also collaborated with partners in numerous European R&D projects related to material qualification and structural material integrity. This includes the Euratom 7th Framework Programme projects MATTER (MATerials TEsting and Rules, 2011-2014) and MatISSE (Materials' Innovations for a Safe and Sustainable nuclear in Europe, 2013-2017), as well as the Euratom Horizon 2020 project PATRICIA (Partitioning And Transmuter Research Initiative in a Collaborative Innovation Action, 2020–2024). In the frame of the GEMMA H2020 project, in addition to material qualification tests in lead environment, the JRC also performed neutron diffraction measurements to determine residual stresses in welded coupons at its High Flux Reactor (HFR) in Petten. These data were used for the validation of welding models in the finite element structural integrity analysis codes.

The JRC Petten as well provides an open access program to its Environmental & Mechanical Materials Assessment (EMMA) Nuclear Research Infrastructure[1]. This includes the AMALIA laboratory, Structural Materials Performance Assessment (SMPA) laboratories, Micro-Characterisation Laboratory (MCL), and Liquid Lead Laboratory (LILLA).

3. SLOW STRAIN RATE TENSILE TESTS OF 316L(N) AND WELDED MATERIAL IN LIQUID LEAD

This section reports on the results of SSRT tests of austenitic stainless steel 316L(N) and its welding joints in liquid lead environment. Because of the combination of their high ductility, mechanical strengths, fracture toughness, and performance under irradiation, austenitic stainless steels of the 316L-type (and its variants) are commonly used for structural components of the sodium-cooled fast reactors [4], and are envisaged for use in LFRs as well.

3.1. Material and methods

3.1.1. SAW 316L(N) welded coupon – material composition

Welded coupons were produced using submerged-arc welding (SAW) technology by Walter Tosto from 75 mm thickness plates of 316L(N) [7]. The geometry of the weld is displayed in Fig. 1.

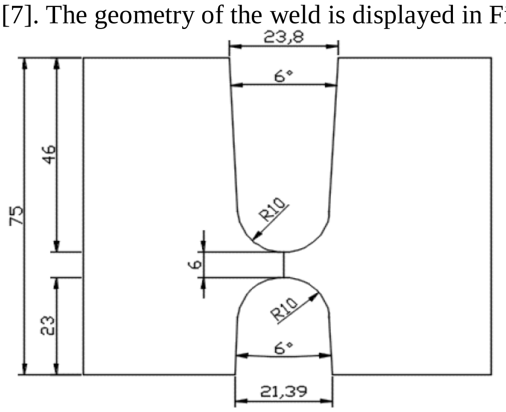

FIG. 1. SAW weld geometry with weld bead shapes and dimensions indicated [7].

The base material was produced by Industeel France (ArcelorMittal) in accordance with the ASME SA-240M (ASTM A240/A240M [8]) specifications. The original plate had dimensions of 1500×4000 mm^2 with a thickness of 75 mm. The plate was solution annealed at 1100-1115 °C for 60 min and then quenched in water (for details cf. [7]). The chemical composition of the plate base metal is given in Table 1. The material corresponds to the specification of the austenitic stainless steel with very-low carbon and controlled nitrogen content, denoted as X2CrNiMo17-12-2(N), 316L(N), and A3.1S group material as given in the RCC-MRx Design Code for nuclear components.

TABLE 1. 316L(N) SAW WELDED COUPON – CHEMICAL COMPOSITION (IN WT.%) OF THE BASE METAL TOGETHER WITH THE MINIMUM AND MAXIMUM RANGES AS STIPULATED IN THE RCC-MRX CODE [4,7].

	C	Si	Mn	P	S	Cr	Ni	Mo	N	B	Cu	Nb	Co
Min	-	-	1.60	-	-	17.00	12.00	2.30	0.060	-	-	-	-
Max	0.030	0.50	2.00	0.025	0.0100	18.00	12.50	2.70	0.080	0.0010	0.30	0.01	0.050
Heat	0.025	0.39	1.72	0.017	0.0008	17.29	12.17	2.40	0.070	0.0007	0.12	0.01	0.024

NB. “-” denotes “not specified”

[1] Cf. https://ec.europa.eu/jrc/en/research-facility/open-access

The selected wire-flux combination for the SAW welded coupon is a Thermanit GE-316L and Avesta Flux 805, respectively. The chemical composition of the weld deposit is displayed in Table 2.

TABLE 2. 316L(N) SAW WELDED COUPON – CHEMICAL COMPOSITION (IN WT.%) OF DEPOSITED WELD MATERIAL [4,7].

	C	Si	Mn	P	S	Cr	Ni	Mo	Nb	N	Co
Min	-	-	1.00	-	-	18.00	11.00	2.00	-	-	-
Max	0.030	1.00	2.50	0.025	0.025	20.00	14.00	3.00	info	info	0.15
Heat	0.015	0.55	1.34	0.016	0.006	19.49	12.16	2.48	0.013	0.053	0.03

NB. “-” denotes “not specified”

The content of ferrite in the deposited weld metal is 11%, which is within the required range of 5-15% [4]. Non-destructive examination of the weld included visual inspection, liquid penetrant examination and radiographic examination. No irregularities or other peculiarities were reported [9].

3.1.2. SAW 316L(N) welded coupon – initial microstructural characterisation

Two specimens were extracted from the cross-section of the 75 mm thick 316L(N) SAW welded plate for electron backscattered diffraction (EBSD) analysis in the scanning electron microscope (SEM) [9]. The obtained inverse pole figure (IPF) maps for the austenite phase can be observed in Figs. 2-4. The rolling direction was perpendicular to the displayed plane.

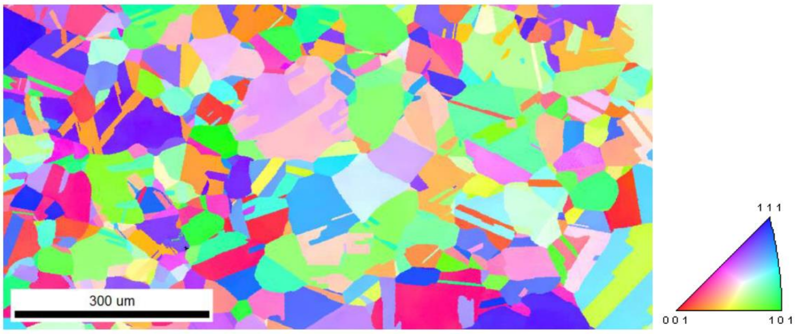

FIG 2. EBSD analysis of the base metal area of SAW 316L(N) welded coupon [9].

The EBSD scan of a characteristic base metal area (1×0.5 mm^2) with 1 µm step-size ca. 8 mm away from the weld line in depicted in Fig. 2. The grains have an average size of ~80 µm and apparently exhibit a random crystallographic texture. A relatively high number of annealing twins are visible within the grains.

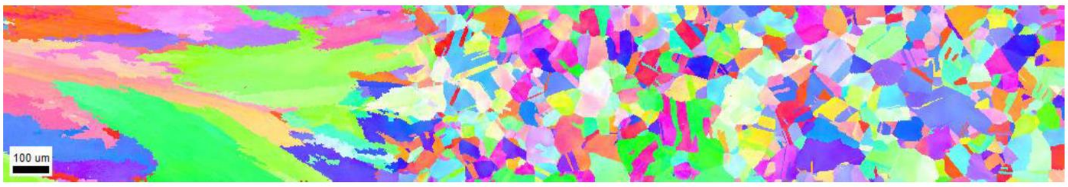

FIG. 3. EBSD analysis of the base metal-weld interface of SAW 316L(N) welded coupon [9].

The EBSD orientation map acquired from the side of the weld including the weld line and the heat affected zone (HAZ) is depicted in Fig. 3. The mapped area size was 3×0.5 mm^2 and an identical scan resolution (i.e., 1 µm) was employed. Large grains within the weld area are visible on the left side of the micrograph. The heat-affected zone, i.e., the notional transition area between the base and weld metal materials, naturally features a wide grain size distribution with no preferential grain size, which gradually decreases towards the base material region. The presence of annealing twins is documented in the recrystallized grains within HAZ.

FIG 4. EBSD analysis of the weld metal area of SAW 316L(N) welded coupon [9].

A larger area (ca. 5×21 mm^2) was also analysed across the weld with a step-size of 10 µm. Fig. 4 displays the resulting EBSD orientation map. The individual weld beads are not clearly distinguished, however, the grooving directions are noticeable. Elongated grains within the weld have a high aspect ratio of 5-10:1. Hence, anisotropy and/or inhomogeneity in the mechanical properties of the weld can be anticipated.

3.1.3. Test matrix and specimens for the SSRT testing

The following specimen geometries were used for SSRT tests:

- Round: ø 2.5 mm, gage length 7.2 mm (cf. Fig. 5) – base metal samples, cut in the longitudinal direction of the coupon;
- Flat: 2 mm x 1.5 mm, gage length 5.6 mm (cf. Fig. 5) – weld metal 90° samples, cut in the transversal direction of the coupon.

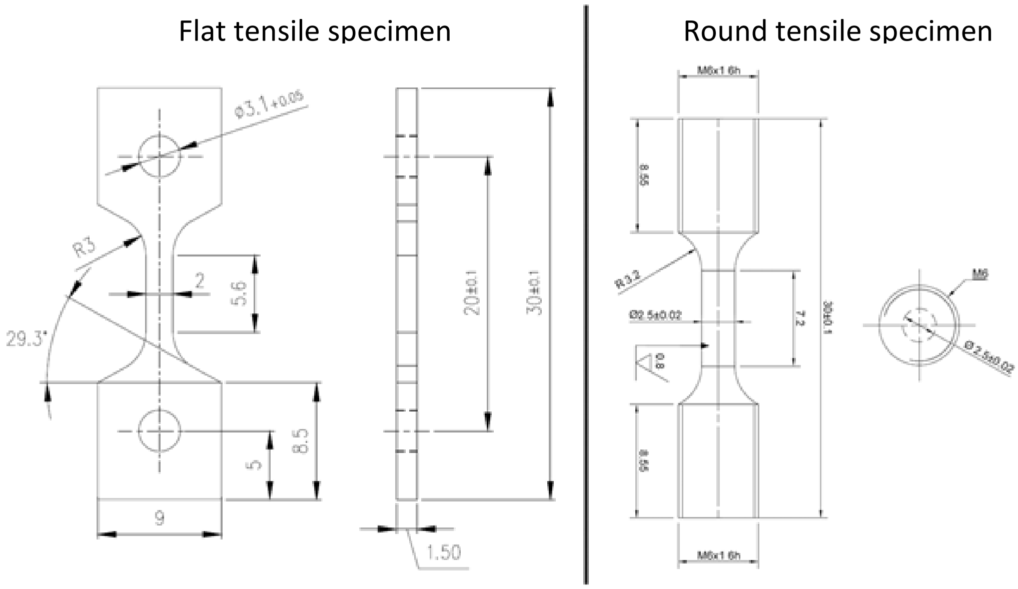

FIG. 5. Specimen shapes and dimensions for the SSRT tests.

The test matrix for the SSRT tests is given in Table 3. The strain rates used for the tests were based on the previous “code of practise” employed by SCK•CEN [10].

TABLE 3. TEST MATRIX FOR THE SLOW STRAIN RATE TESTS.

Temperature	**Strain rate [s^{-1}]**	**Zone**	**Environment**
400 °C	$5{\cdot}10^{-5}$	Base metal	Ar and Pb
400 °C	$5{\cdot}10^{-5}$	Weld metal (90°)	Ar and Pb
550 °C	$5{\cdot}10^{-6}$	Base metal	Ar and Pb
550 °C	$5{\cdot}10^{-6}$	Weld metal (90°)	Ar and Pb

Tensile tests in Ar were performed as a reference for the tests performed in liquid Pb.

Pre-test conditions for the specimens followed the GEMMA-recommended specifications to perform the pre-exposure in molten Pb for at least 30 hours at 500 °C with the oxygen content below 10^{-8} wt.%.

3.1.4. The LILLA facility

The LILLA experimental facility consists of two cylindrical tanks: a measuring tank and storage tank that are connected by piping to transfer liquid lead between the tanks [2]. A 3D drawing and an actual photograph of the facility are displayed in Fig. 6.

The main characteristics of the LILLA facility are:

- Operating temperatures in lead: up to 650 °C;
- Operating range of oxygen concentrations in lead: from saturation to less than 10^{-10} wt.%;
- Lead inventory: ca. 35 l;
- Surfaces in contact with molten lead are protected by Al_2O_3 coating (using the pack cementation technology);
- Active control of gas/oxygen injected to cover gas space and to molten lead (below surface) by an appropriate admixture and delivery of Ar, Ar-H_2, and synthetic air to the facility;
- Up to four test sections (with a possibility to conduct four corrosion-mechanical tests independently);
- Two reserve ports (diameter 35 mm) with a possibility for multiple feed-throughs.

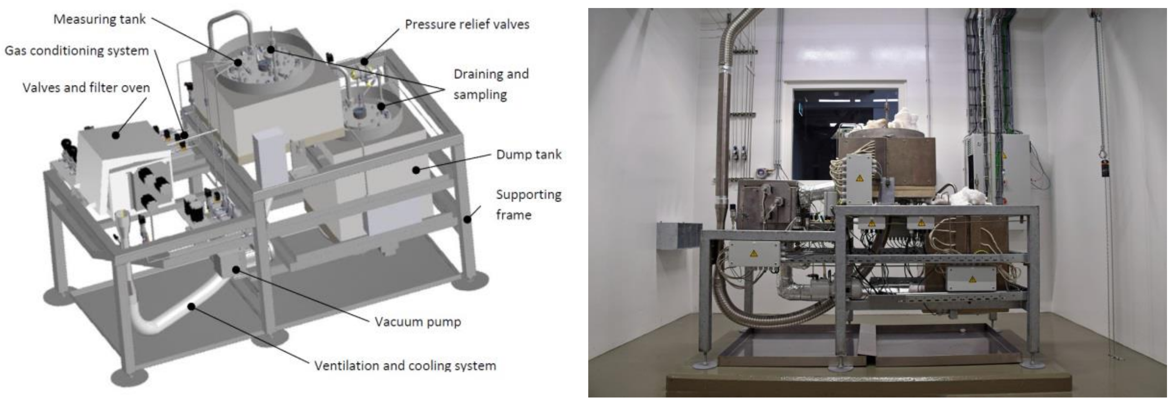

FIG. 6. Drawing (left) and view (right) of the LILLA experimental facility for material testing in liquid lead.

As a special feature of the LILLA facility, the natural convection flow of lead in the measuring tank can be regulated through varying the power of external heaters and heat losses to an internal cooling channel. This feature facilitates a time-efficient distribution and control of the oxygen dissolved in liquid lead. Electrochemical sensors based on the yttria-stabilised zirconia(YSZ)/Pt(air) reference electrode are used to monitor and actively control the oxygen content in lead.

The test section load is generated by a new type of the pneumatically-driven double2bellows (D2B) devices, see Fig. 7. Both tensile and compressive loads can be generated. The four test sections are independent and have the following main characteristics:

- Maximum load: 12 kN, push/pull;
- Operating range of strain rates: 10^{-9} to 10^{-2} s^{-1};
- Test / hold times: up to at least 1000 h.

Test sections are equipped with a detachable fixing system for various test and specimen types, see Fig. 8. A wide range of tests, including SSRT tests, fracture toughness tests, crack growth rate tests, and small punch tests are possible.

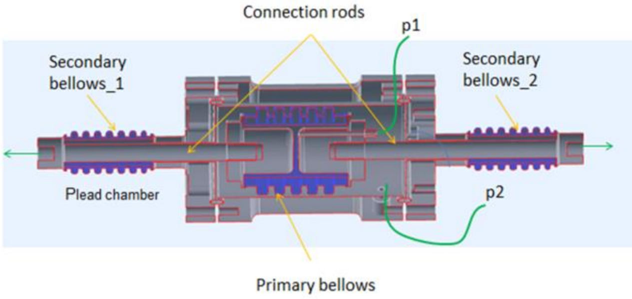

FIG. 7. The double2bellows (D2B) loading device.

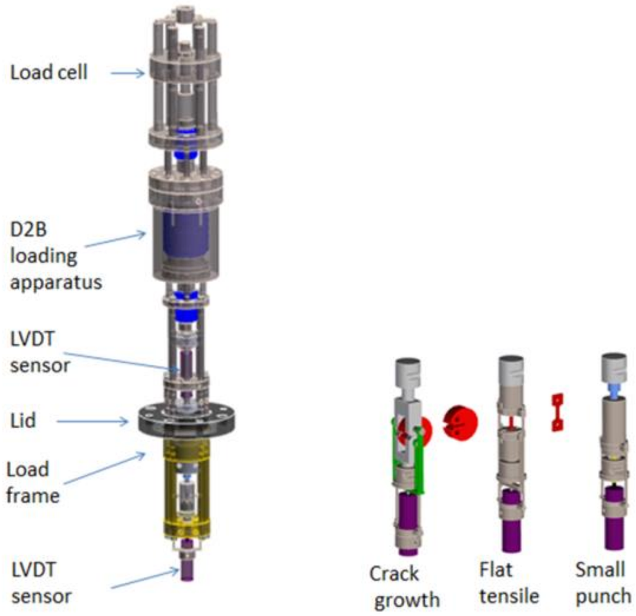

FIG. 8. Main parts of the test section together with the fittings for the crack growth/fracture toughness, tensile, and small punch tests.

3.1.5. Post mortem microstructural investigation

The fracture surfaces were examined in the optical stereomicroscope (in the magnification range from 4 to 70 times), and in the SEM (in the magnification range from 20 to 20000 times). The specimens were cleaned in the acetone bath prior to fractographic analysis in SEM. A basic SEM photo-documentation of fracture surface was realised, in the form of sets of micrographs at magnifications 50×, 100×, 300×, 1000×, 3000×, and 10000×. The photo-documentation was acquired using the secondary electron (SE) signal as well as the backscattered electron (BSE) signal. The same procedure was used for the observation and photo-documentation of specimens' lateral walls in the vicinity of the fracture surfaces.

After the observation of (as-received - uncleaned) fracture surfaces and lateral walls, the specimens were repeatedly cleaned in the solution of $CH_3COOH+C_2H_5OH+H_2O_2$ (1:1:1). After each step of cleaning, a basic SEM observation and photo-documentation of fracture surfaces were realised.

One half of each fractured specimen was longitudinally cut by thin diamond saw approximately in the middle of the specimen and the metallographic cut was prepared by the standard procedure (embedding in the conductive resin, grinding, and polishing with final step in 0.05 μm colloidal silica). The observation of the metallographic cuts was carried out in the magnification range from 25 to 1000 times using the light microscope (in normal incident and polarised light mode), and in the magnification range from 20 to 10000 times using the SEM. For the light microscopy (grain structure characterization), the samples were etched in the solution of $HCl+HNO_3+H_2O$ (1:1:1).

3.2. Results of the SSRT tests

The SSRT tests performed at the JRC on the sub-sized samples from the 316L(N) SAW welded coupon were carried out in Ar or in liquid Pb environment at elevated temperatures according to the test matrix presented in Section 3.1.3 and Table 3. The engineering stress-strain curves for all combinations of testing conditions are shown in Figs. 9 and 10.

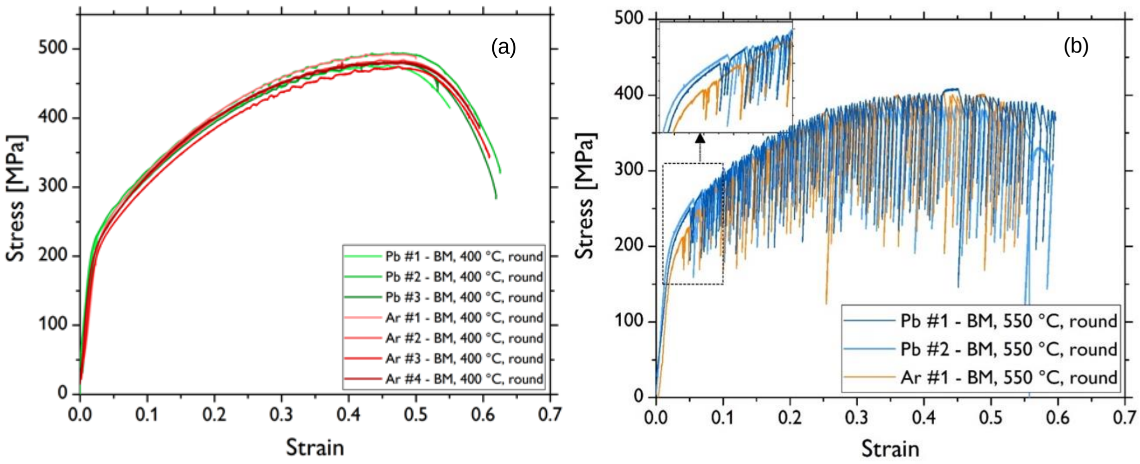

FIG. 9. Tensile curves of 316L(N) SAW base metal material at: (a) 400 °C; and (b) 550 °C.

Fig. 9a shows the representative engineering tensile curves of SSRT tests carried out on base metal samples in liquid Pb and in Ar at 400 °C, whereas the tests at 550 °C are shown in Fig. 9b. The outcomes of the experiments show a good repeatability and similar mechanical response in both Ar and Pb. Serrated plastic flow is observed on base metal samples at both 400 °C and 550 °C, most probably due to dynamic strain ageing (DSA) as also reported elsewhere [12-14]. The serrations are more pronounced at 550 °C.

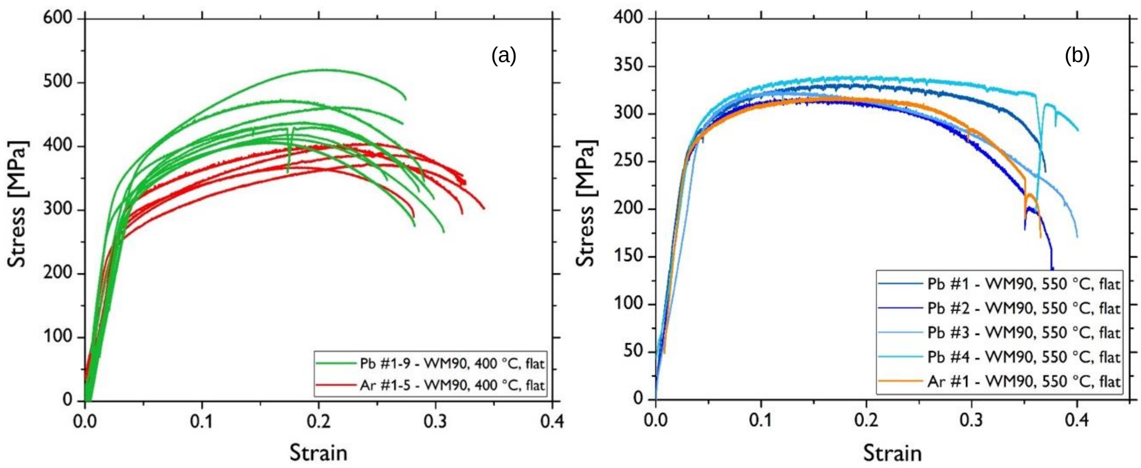

FIG. 10. Tensile curves of 316L(N) SAW weld metal 90° material at: (a) 400 °C; and (b) 550 °C.

The results of SSRT tests on the weld metal 90° samples are presented Fig. 10a (at 400 °C) and Fig. 10b (at 550 °C). Due to the inherent microstructural inhomogeneities of the weld metal material (see also Section 3.1.2), the tests repeated at the same conditions (temperature and strain rate) exhibit larger scatter. However, some general trends can be observed: tests conducted in Pb show indications of somewhat higher flow stress (both yield point and ultimate tensile stress) and slightly lower ductility compared to the tests performed in Ar. Similar propensities are also observed in the case of SSRT tests on the weld metal 90° samples at 550 °C. Analogues scatter in the tensile data was also experienced when the weld metal 90° samples were tested in the (reference) air atmosphere, cf. Fig. 11.

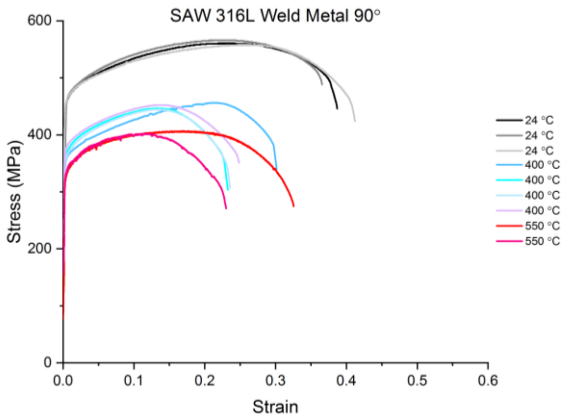

FIG. 11. Tensile curves of 316L(N) SAW weld metal 90° material – SSRT tests at room and elevated temperatures in air. Due to inherent microstructural inhomogeneities, larger scatter of results is observed, in particular at 400 °C (four tests) and 500 °C (two tests).

3.3. Post-mortem microstructural observations

Fig. 12 shows the complementary post-mortem microstructure observations for one of the base metal specimens tested in liquid Pb at 550 °C. The side view of a sample surface (Fig. 12a) shows ductile fracture in terms of the apparent lateral contraction (ductile necking before the failure). This finding is supported by the presence of ductile dimples on the fracture surface (Fig. 12b). The cross-section along the testing axis is displayed in Fig. 12c, which shows elongated grains in the loading direction. The SEM micrograph depicting the detail of the microstructure and interface between the sample and liquid lead is shown on Fig. 12d. No liquid Pb interaction (depletion of alloying elements and/or Pb penetration by diffusion) could be inferred from the micrographs. On the other hand, the microstructure is heavily deformed - dislocation slip activity is visible in the sample interior as well as on the sample surface in the form of deformation bands.

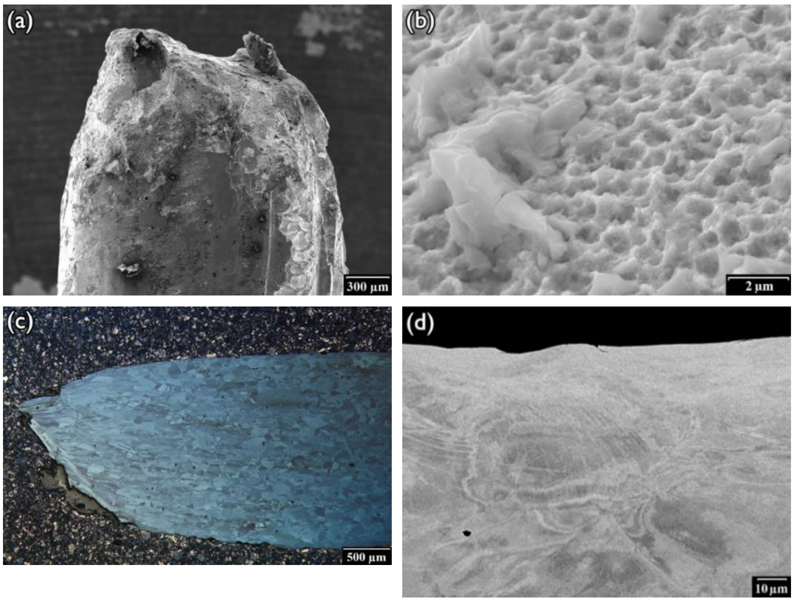

FIG. 12. Complementary post-mortem SEM observation of the base metal specimen tested at 550 °C in liquid Pb: (a) side view of the specimen after fracture (SE signal); (b) detail of fracture surface (SE signal); (c) cross-section along the loading axis (light microscopy in the polarised light); and (d) detail of cross-section and interfacial microstructure (BSE signal).

The microstructure of one of the weld metal 90° specimens after an SSRT test at 400 °C is depicted in Fig. 13. Ductile fracture is also observed here as both lateral contraction and dimples are evidenced by the micrographs (Fig. 13a,b). However, in this case, the longitudinal cross-section (Fig. 13c,d) shows a dendritic structure typical of austenitic steel welds as a result of high cooling rates during welding [15]. Nevertheless, no clear indications of liquid Pb interaction with the weld 90° material are observed (Fig. 13e,f).

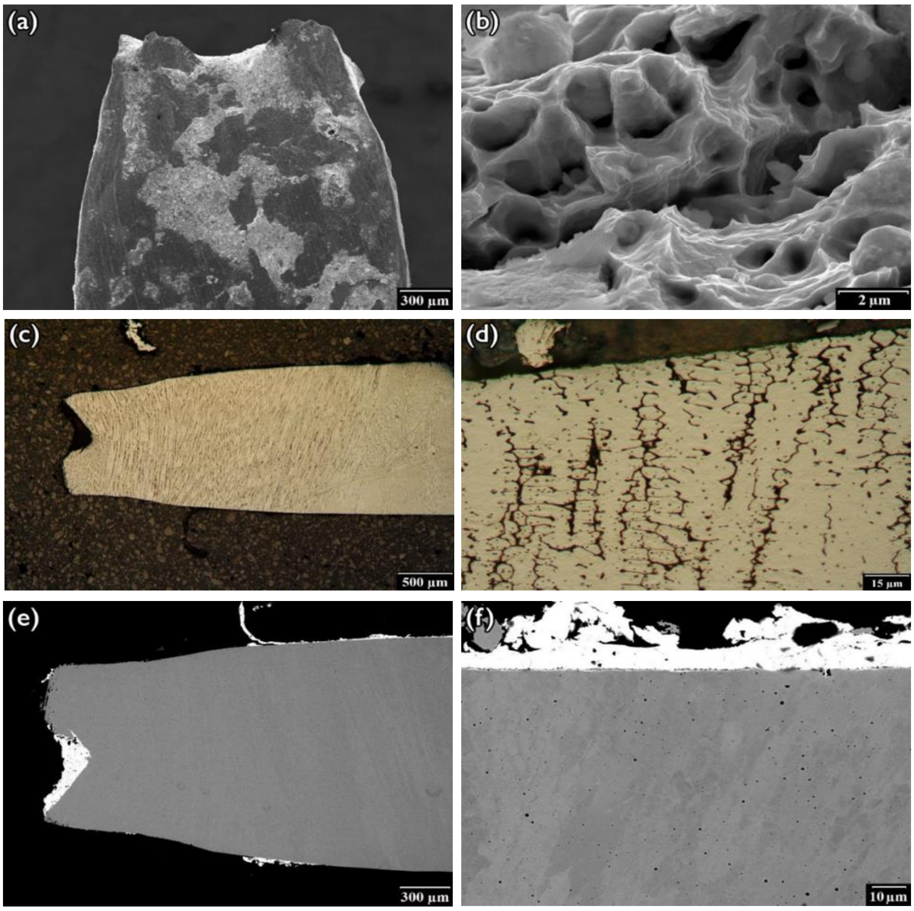

FIG. 13. Complementary post-mortem SEM observation of a weld metal 90° specimen tested at 400 °C in liquid Pb: (a) side view of the specimen after fracture (SE signal); (b) detail of fracture surface (SE signal); (c) cross-section along the loading axis (light microscopy in the bright field); (d) zoomed-in (c) image; (e) detail of cross-section and interfacial microstructure (BSE signal); and (f) zoomed-in (e) image.

3.4. Discussion

During the SSRTs performed on the material from the SAW 316L(N) welded coupon, the base metal specimens exhibited, under the chosen test conditions, and at both 400 °C and 550 °C, practically identical tensile behaviour when tested in Ar and liquid Pb. This is in line with the observations reported earlier on the tensile behaviour of 316L-grade steels in lead-bismuth eutectic [10,16] and by other GEMMA partners, who conducted tests both in Pb and LBE [11]. On the other hand, due the observed inhomogeneous weld microstructure, the inherent scatter in the measured tensile data prevents drawing any robust conclusions for behaviour of the weld metal 90° material. Nevertheless, the measured tensile curves seem to indicate some tendency to having a slightly lower flow stress and higher elongation when tested in Ar in comparison with tests in liquid Pb (especially at 400 °C). The basic microstructure observations bear witness of ductile fracture, and there are no indications of liquid metal embrittlement and/or environmental-assisted cracking on fracture surfaces and/or lateral walls of all analysed specimens.

4. CONCLUSIONS

This paper summarizes activities of the JRC Petten in the domain of structural material integrity for LFRs. It thereafter describes the results of slow-strain rate tensile tests of 316L(N) and its SAW welded joints in oxygen-controlled liquid lead environment. At the studied experimental conditions, the current research results did not reveal any indications for the existence of liquid metal embrittlement and/or environmental-assisted cracking of 316L(N) in liquid lead. Together with other GEMMA partners' results, this research supports resolution of key safety and licensing aspects for MYRRHA and ALFRED LFRs.

ACKNOWLEDGEMENTS

The authors wish to acknowledge all collaboration organisations in the area of LFRs and structural integrity research for advanced reactor systems. The support of PneMo and the Czech Technical University in conducting this research is also gratefully acknowledged. The research leading to these results has been partly carried out in the frame of the Joint Programme on Nuclear Materials of the European Energy Research Alliance (EERA JPNM) and funded by the Euratom research and training programme 2014-2020 under grant agreement No. 755269.

REFERENCES

[1] ALEMBERTI, A. et al., Lead-cooled Fast Reactor (LFR) System Safety Assessment, Generation-IV International Forum (GIF), June 2021.

[2] TUČEK, K, et al., "Tensile testing of sub-sized T91 steel specimens in liquid lead", In Proceedings of a Technical Meeting on Structural Materials for Heavy Liquid Metal Cooled Fast Reactors, IAEA-TECDOC-1978, 2021.

[3] AGOSTINI, P., et al., GEMMA: GenIV Materials Maturity, Euratom H2020 collaborative project (Grant Agreement no. 755269), In Proceedings of 9th European Commission Conference on Euratom Research and Training in Safety of Reactor Systems − FISA 2019, European Commission, Brussels, 2020.

[4] MUÑOZ GARCIA, J.E., et al., Design and construction rules for mechanical components of high-temperature, experimental and fusion nuclear installations: the RCC-MRx Code last edition, Mechanical Engineering Journal, Vol. 7(4), paper no. 20-00052, 2020.

[5] MALERBA, L., BERTOLUS, M., NILSSON, K.-F., Materials for sustainable nuclear energy, The Strategic Research Agenda (SRA) of the Joint Programme on Nuclear Materials (JPNM) of the European Energy Research Alliance (EERA), JRC116292, EUR 29740 EN, Luxembourg: Publications Office of the European Union, 2019.

[6] GIF, Safety Design Criteria for Generation IV Lead-cooled Fast Reactor System, GIF LFR pSSC in collaboration with RSWG, 2021.

[7] BARBIERI, G., Weld specimen specifications and characterisations, Deliverable D2.1, Rev. C, GEMMA Euratom H2020 Project No. 755269, June 2020.

[8] ASTM, Standard Specification for Chromium and Chromium-Nickel Stainless Steel Plate, Sheet, and Strip for Pressure Vessels and for General Applications, ASTM A240/A240M, 2020.

[9] SERRANO, M., Characterization of mechanical properties and microstructure of reference welds in air, Deliverable D2.3, GEMMA Euratom H2020 Project No. 755269, March 2020.

[10] STEFANINI, L. et al., "Investigation of Liquid Metal Embrittlement of AISI 316L steels", In Proceedings of the 24th International Conference on Nuclear Engineering, ICONE24, Charlotte, North Carolina, USA, June 26-30, 2016.

[11] NILSSON, K.-F. et al., Effect of liquid lead on mechanical properties of austenitic steels, their welds and implications for design, Deliverable D4.7, GEMMA Euratom H2020 Project No. 755269, November 2021.

[12] GANESAN, V. et al., Effect of nitrogen content on dynamic strain ageing behaviour of type 316LN austenitic stainless steel during tensile deformation, Materials at High Temperatures, vol. 31, no. 2, pp. 162–170, May 2014.

[13] MUHAMED, G. et al., Dynamic Strain Aging Behaviour in AISI 316L Austenitic Stainless Steel under As-Received and As-Welded Conditions, Metals, vol. 7, no. 9, p. 362, September 2017.

[14] EHRNSTÉN, U. et al., Dynamic Strain Ageing of Deformed Nitrogen-alloyed AISI 316 Stainless Steels, In Proceedings of the 12th International Conference on Environmental Degradation of Materials in Nuclear Power System – Water Reactors, p. 10, Salt Lake City, UT, USA, 2005.

[15] WU, C. et al., Microstructural evolution in 316LN austenitic stainless steel during solidification process under different cooling rates, J Mater Sci, vol. 51, no. 5, pp. 2529–2539, March 2016.

[16] FAZIO, C. et al., Handbook on Lead-bismuth Eutectic Alloy and Lead Properties, Materials Compatibility, Thermalhydraulics and Technologies, 2015 Edition, NEA. No. 7268, Nuclear Energy Agency, Paris, France, 2015.